fDOI: 10.1002/ ((please add manuscript number))
Full Paper

A Robust Design for Cellular Vehicles of Gold Nanorods for Multimodal Imaging

Fulvio Ratto, Sonia Centi, Cinzia Avigo, Claudia Borri, Francesca Tatini, Lucia Cavigli, Claudia Kusmic, Beatrice Lelli, Sarah Lai, Stefano Colagrande, Francesco Faita, Luca Menichetti and Roberto Pini*

Dr F. Ratto, Dr S. Centi, Dr F. Tatini, Dr L. Cavigli, B. Lelli, Dr S. Lai, Dr R. Pini
Institute of Applied Physics 'N. Carrara', National Research Council Italy, via Madonna del Piano 10, 50019 Sesto Fiorentino (FI), Italy
E-mail: f.ratto@ifac.cnr.it
C. Avigo, Dr C. Kusmic, Dr F. Faita, Dr L. Menichetti
Institute of Clinical Physiology, National Research Council Italy, via Moruzzi, 1, 56124 Pisa (PI), Italy
Dr C. Borri, Prof S. Colagrande
Department of Experimental and Clinical Biomedical Sciences 'M. Serio', University of Florence, largo Brambilla 3, 50134 Firenze (FI), Italy

Keywords: gold nanoparticles; macrophages; chemotaxis; photoacoustic imaging; X-ray computed tomography

The pursuit of more selectivity in the delivery of plasmonic particles to tumors is critical before their penetration into clinical applications as the photoacoustic imaging and the photothermal ablation of cancer. As their direct infusion into the bloodstream remains problematic, due to a multitude of biological barriers, the development of alternative approaches is emerging as a new challenge. In this context, the recruitment of homologous tumor-tropic cells that may serve as Trojan horses stands out as a fascinating possibility. Here, we present a novel model of gold nanorods that feature a composite shell and undergo efficient and reproducible endocytic uptake from murine macrophages, which is fine-tunable over a broad range of conditions. These cells preserve their viability and more than 90% of their innate chemotactic behavior in vitro, even with a cargo exceeding 200˙000 particles per cell. In addition, we show that these vehicles are detectible by photoacoustic imaging down to concentrations in the order of 1% in whole blood and by clinical CT below 10%, which is within the typical fraction of a leukocytic infiltrate in a tumor microenvironment, and may even work as contrast agents for the photothermal ablation of cancer.

1. Introduction

The clinical exploitation of plasmonic particles such as gold nano-rods, shells, cages and other nonspherical shapes has become a remarkable mission for a willful community of scientists[1-6]. These particles are being proposed as contrast agents for various applications in biomedical optics, including the photothermal ablation and the photoacoustic imaging (PAI)[7, 8] of cancer, which are emerging as hopeful alternatives in oncology. A favorable premise of gold nanoparticles is their good tolerability in vivo[9-11]. Moreover, at variance with gold nanospheres that resonate in the green as many biological dyes including hemoglobin, the particular shapes of gold nano-rods, shells and cages originate new bands of optical absorbance in the near infrared (NIR)[12], which is ideal to achieve high penetration and contrast in bio-tissue. In particular, the plasmonic bands of gold nanorods are tunable across the entire window of the NIR with their size and shape and provide for unique cross sections of optical absorbance[5, 13-15]. Their efficiency of photothermal conversion outclasses that of organic dyes by several orders of magnitude and also that of alternative gold nanoparticles[16, 17]. Another advantage over organic dyes is the stability of these cross sections in biological fluids. However, new pitfalls are hidden at the interface with cells[9]. For instance, as gold nanoparticles undergo endocytic uptake, their aggregation within tight vesicles may jeopardize their optical features[18-20], due to plasmonic coupling. Different authors have proposed the use of rigid shells such as silica as a spacer to prevent this warning[19, 21]. Indeed, floccules of silanized gold nanorods in anhydrous biopolymers retain most of their optical features, while softer shells such as polyethylene glycol (PEG) are ineffective[18]. However, while inorganic shells may provide new functions[22, 23], we found a different scenario in endocytic vesicles. There, we noted that PEG strands of the appropriate weight are enough to inhibit plasmonic coupling[24]. In essence, whereas PEG shells collapse in anhydrous

environments, their steric hindrance works well in moist conditions, even at extreme concentrations. In addition, the colloidal stability of PEGylated gold nanorods in biological fluids is critical for the feasibility of their tests in vitro and in vivo[25, 26].

At present, one of the most relevant challenges in nanomedicine is to really optimize the delivery of functional nanoparticles into tumors upon systemic administration, as a magic bullet. In this context, PEGylated gold nanorods are a hopeful platform. Their hydrodynamic size is ideal to passively pervade tumors that exhibit enhanced vascular permeability and poor lymphatic drainage[10, 27-29]. Besides, PEG strands and other spacers holding reactive moieties enable their bio-conjugation with targeting units that actively bind malignant phenotypes[20, 24, 30, 31]. PEGylated and bio-conjugated gold nanorods display high specificity and blood compatibility in vitro[30]. Therefore, their direct injection into the bloodstream has become a mainstream solution. However, after more than one decade of preclinical trials in dozens of labs, this route still remains problematic. Upon intravenous injection, more than ~ 90% of the gold nanorods typically get captured by the mononuclear phagocyte system (MPS)[4, 10, 32, 33]. Indeed the complexity of the biological barriers in a full body[34], comprising the MPS, the vessel walls, the tumor stroma, etc. poses a formidable challenge to really optimize the design of these particles.

More recently, the notion to exploit the natural tropism of cells such as tumor-associated macrophages[35-39], T cells[40], mesenchymal stem cells[41-43] and neural stem cells[44, 45] has begun to emerge as a radical alternative. These cells hold an innate ability to detect and to infiltrate tumors with high specificity[46-49], with the aim to modulate their microenvironment in a variety of ways. In particular, macrophagic infiltrates are common in cancer as well as in atherosclerosis, myocardial infarction, aortic aneurysm, diabetes and other conditions and are emerging as a new target for imaging and treatments[50-54]. In most tumors, the extent of macrophagic infiltrates correlates with a poor prognosis and may exceed 50% of their size[55-57]. These macrophages accumulate even in hypoxic and necrotic segments, stimulate the

angiogenesis, support the malignant cells in terms of invasion, motility, intravasation in primary sites and of extravasation, survival and persistent growth in metastatic sites, prime premetastatic sites and also play an immunosuppressive role, by protecting the malignant cells against natural killer and T cells[47]. In turn, tumor-associated macrophages may be conceived of as Trojan horses to take up and to deliver functional cargos to their biological target, including plasmonic particles such as gold nanoshells[35-39]. Several authors have suggested that this approach may improve the distribution and retention of different particles both in malignant against normal tissue[36, 40, 42] and within malignant tissue[43-45]. Other advantages include a full personalization of the treatment and a remarkable simplification of the biological interface.

In essence, the design of gold nanorods needs to provide for their efficient uptake from macrophagic cells that maintain their viability and tropism. Over recent years, Vigderman et al[58] and Schnarr et al[45] have shown that quaternary ammonium compounds are capable to drive a massive uptake of gold nanorods into endocytic vesicles, due to their positive zeta potential[59]. Here, we combine this notion with the observation that cell penetrating agents with a cationic profile[60, 61] preserve their functionality after inclusion within PEG shells[62], which add colloidal stability and biocompatibility[25,26]. We propose a novel design of polycationic gold nanorods that enable a robust fabrication of cellular vehicles. We demonstrate their viability and tropism and their use as contrast agents for PAI and CT even in whole human blood in a tissue-like optical phantom down to concentrations of a few percent, which is at least an order of magnitude below the typical extent of macrophagic infiltrates in tumors.

2. Results and Discussion

2.1. Polycationic Gold Nanorods

As it is discussed in Experimental Section, gold nanorods were PEGylated and then saturated with (11-Mercaptoundecyl)-N,N,N-trimethylammonium bromide (MUTAB) in one pot, in order to achieve polycationic particles. Their zeta potential was (20 ± 2) mV, which is attributed to the permanent charge of the quaternary ammonium moieties of MUTAB. As a reference, this value dropped to (-18 ± 2) mV when MUTAB was replaced with 11-Mercaptoundecanoic acid, which only differs from MUTAB by the substitution of the quaternary ammonium end with a C-terminus. The zeta potential of polycationic gold nanorods from different batches within a range of aspect ratios from ~ 3.0 to ~4.5 and effective radii around 10 nm was found to differ from each other by less than ±10%. The colloidal stability of these particles proved to be optimal even after at least five cycles of centrifugation and dispersion in phosphate buffered saline (PBS) and various culture media up to gold contents around 80 mM Au, which is about the PEG shells. We note that, when we tried to modify gold nanorods with MUTAB in the absence of PEG, as in Schnarr et al[45] and Mooney et al[44], particles began to flocculate in PBS soon after the first cycle of centrifugation, which would be a major concern for the reproducibility of their applications.

2.2. Plasmonic macrophages: optical features

Murine macrophages were incubated with different concentrations of polycationic gold nanorods over different times. **Figure 1** and **S1** report representative micrographs of macrophages treated for 24 hrs with 400 μM Au. The presence of a dark particulate within the perinuclear cytoplasm is already visible by the use of an optical microscope, as it is seen in **Figure S1**. On closer inspection by the use of electron microscopy, gold nanorods are seen to undergo tight confinement within endocytic vesicles that exhibit a broad range of sizes in the

order of a few hundred nm and distances of a few µm, which is consistent with the findings from other authors[20, 45, 58, 59].

On visual inspection, the pellets of these cells became darker and darker both with the increase of incubation dosage and time. In an attempt to quantify the underlying kinetics, these pellets were fixed, re-suspended in PBS and directed to an optical analysis. Their spectra of optical extinction revealed the same plasmonic bands as the original suspensions of gold nanorods, with minimal modifications (see **Figure S2**), which implies the absence of significant plasmonic coupling. Their lineshapes were modeled as the sum of an empirical background from an unknown number of cells, which was calibrated in a preliminary measurement, plus a numerical approximation of the plasmonic band from an unknown number of gold nanorods. The latter was devised as a convolution integral between Gans lineshape[15, 63, 64], which was implemented with the dielectric function by Etchegoin et al[65], and an unknown distribution of aspect ratios. Details and a demonstration of this method are reported elsewhere[24, 63, 64]. The output of this analysis is a number of particles per cell. Results are displayed in **Figure 2**. The number of particles per cell is linear with incubation dosage and undergoes exponential saturation with incubation time. In particular, after 24 hrs, the effective rate of uptake per unit of incubation dosage is (580 ± 40) particles / cell / µM Au. In turn, with an incubation dosage of 400 µM Au, the initial rate of uptake per unit of incubation time is (260 ± 50) particles / cell / min. In practice, macrophages treated for 24 hrs with 400 µM Au contain as many as ~200˙000 gold nanorods. These figures are in the same order of magnitude as the records that were reported by Vigderman et al[58], when it is considered that macrophages are smaller than other kinds of cells. However, at variance with the use of particles without PEG, where the uptake of gold was found to vary from replica to replica by as much as a factor of ~3˙000%[44] under identical conditions, we verified that our protocol is reproducible within ± 20%. This dramatic improvement is attributed to the

colloidal stability that belongs to the steric hindrance of PEG. In addition, this hindrance persists even in the extreme densities of the endocytic vesicles, which is demonstrated by the near-absence of plasmonic coupling in the spectra of optical extinction in **Figure S2**.

2.3. Plasmonic macrophages: viability and tropism

Perhaps, the most critical concern for the preparation of cellular vehicles is about the preservation of their biological functions of interest. Both the optical and the electron micrographs of our macrophages reveal that their morphology remains normal upon interaction with polycationic gold nanorods, which points to an overall conservation of their physiology.

Figure 3a displays the viability of these cells upon incubation with cationic gold nanorods. A modest decrease is seen both with the incubation dosage and time, which is more likely to result from a reduction of cell proliferation rather than the onset of apoptosis or necrosis, according to our optical micrographs. After incubation for 24 hrs with 400 μM Au, the viability is still within ~10% of control. Therefore we conclude that no significant cytotoxic effect is detectible within the range of conditions that was explored.

Figure 3b shows the migration of macrophages treated with 100 and 400 μM Au for 24 hrs with respect to controls in the presence and absence of a chemotactic stimulus, such as a gradient of MIP-1α[66]. We emphasize that these cells were first prepared with polycationic gold nanorods and then tested for their chemotactic migration, as it would occur in a real-world application. Also this parameter keeps satisfactory.

Blank cells exhibit a very low level of motility in serum-free medium without chemokine. Likewise, the treatment with gold nanorods alone does not trigger their chemotaxis, thus demonstrating that these particles are unable to activate murine macrophages. Conversely, their incubation with MIP-1α (50 ng/ml) exerts a sharp increase in their chemotaxis. More

than 90% of this migration is still observed in macrophages that were pre-treated with 100 and 400 µM Au and then exposed to MIP-1α. Therefore, our polycationic gold nanorods do not inhibit the chemotaxis of murine macrophages under these conditions.

These results are in line with those by Schnarr et al[45] and Madsen et al[38] and suggest that the chemotactic functions of macrophages are robust in the presence of nontoxic gold nanoparticles.

Overall, our macrophages maintain well their viability and tropism in vitro, which is their principal functions in view of their use as Trojan horses.

2.4. Plasmonic macrophages: contrast for biomedical imaging

The possibility to map macrophagic infiltrates of cells treated with polycationic gold nanorods was addressed by PAI. These cells are tested as exogenous agents to enhance the optical contrast by their plasmonic cargo and to break through the imaging-depth limit. With this approach, the excitation of the plasmonic oscillations of gold nanorods with short optical pulses triggers a cascade of photothermal and thermoelastic conversion in their fluid environment, which leads to the emission of ultrasound[7, 8]. Here, we combined a high resolution photoacoustic and micro-ultrasound platform that operates in the range of wavelengths between 680 and 970 nm and a linear array transducer. As for the samples, we used a tissue-like optical phantom to achieve semi-quantitative data from sets of micro-channels drawn in a polymeric scaffold. Meanwhile, owing to the large atomic number of gold, we investigated the possibility to detect our macrophages with a microCT scanner.

The fingerprint of plasmonic macrophages was detected by the use of photoacoustic spectroscopy[67, 68]. First, we recorded the photoacoustic signals from micro-channels that were filled with aqueous suspensions of gold nanorods without cells. These data are reported in **Figure S3** and reveal that the plasmonic bands of these samples are retraced well down to

concentrations in the range of ~ 100 µM Au. The intensity of the photoacoustic signals undergoes exponential saturation with the dosage of gold, as the optical fluence becomes more and more exhausted by the particles, which was used to establish a calibration curve. Next, the micro-channels were filled with ~10^7 plasmonic macrophages per cc. In this case, the shape of the photoacoustic spectra departs a little further from that of the optical extinction, which we ascribe to the onset of nonlinear effects, such as cavitation[68, 69], that grow up in the extreme densities of the endocytic vesicles[70, 71]. Nonetheless, the intensity of the photoacoustic signals still scales with the number of particles per cell and fits rather well in the calibration curve, when the data from **Figure 2** are worked out into the overall content of gold in these samples. All this data demonstrates that macrophages treated for 24 hrs with 100 to 400 µM Au are discriminated well from a background of PBS even at a concentration of ~1% (v/v), which is at least an order of magnitude below the typical fraction of the macrophagic infiltrate in a malignant lesion.

The same applies to whole blood as well. **Figure 4a** and **4b** show photoacoustic spectra and a representative photoacoustic image of three micro-channels that were filled with human whole blood, a suspension of gold nanorods in whole blood at the concentration of 1 mM Au and whole blood containing ~3% (v/v) macrophages treated for 24 hrs with 400 µM Au. The photoacoustic spectra of whole blood display the typical fingerprint of oxygenated hemoglobin[72, 73]. In addition to this fingerprint, the plasmonic band of gold nanorods dominates in both other samples and its intensity scales well with the concentration of gold, when it is considered that ~3% (v/v) macrophages treated for 24 hrs with 400 µM Au amounts to (2.3 ± 0.5) mM Au. **Figure 4a** demonstrates that the detection limit of the plasmonic macrophages in whole blood falls well below 3% (v/v), which substantiates the feasibility of this approach in vivo.

In order to understand the possibility to image the accumulation of these cells even deeper inside bio-tissue, we verified the contrast of gold nanorods by conventional CT from relevant inclusions of a volume of ~100 µL. **Figure S4** displays our calibration curve. At variance with the previous work by von Maltzahn et al[17], we focused on a regime of lower concentrations of gold, which may be accessible by the use of cellular vehicles. In this regime, upon optimization of the setup, the absorbance is linear with the concentration of Au with a rate of (16 ± 2) H.U. / mM Au.

Figure 4c displays a CT image of a set of inclusions containing standard solutions of iodine in PBS, suspensions of gold nanorods in PBS at the concentration of 4 mM Au, and ~8% (v/v) macrophages treated for 24 hrs with 400 µM Au. We note that the latter is still well below the possible content of tumor-associated macrophages in a malignant lesion. Therefore, the combination of **Figure 4b** and **4c** illustrates the potential of our cells as contrast agents for a multimodal approach of biomedical imaging.

In addition to their value for biomedical imaging, another major field of application for gold nanoparticles is the photothermal ablation of cancer[17, 74-77]. In this context, the same plasmonic oscillations of gold nanorods that provide for optical contrast for PAI are activated with a continuous wave in order to raise the temperature of their medium above the physiological value. **Figure S5** shows that, upon excitation with a continuous wave under conditions that are harmless to blank macrophages, those treated for 24 hrs with 400 µM Au undergo lethal damage within a few minutes. What is more, a monolayer of these cells is already sufficient to overheat their microenvironment above ~65°C (max continuous service temperature of polystyrene), as it is inferred from their effect on the Petri dish. Therefore, in addition to their value as multimodal agents of contrast for biomedical imaging, these cells hold the potential to serve as microradiators for the photothermal ablation of cancer.

3. Conclusion

In conclusion, we have disclosed a new model of gold nanorods that combine strong cationic profiles and colloidal stability, by the development of a composite shell of quaternary ammonium compounds and PEG. These particles undergo efficient and reproducible uptake from tumor-tropic cells such as macrophages, which preserve their viability and more than 90% of their innate chemotactic behavior in vitro. The amount of particles per cell is fine-tunable with the parameters of their co-incubation, at least until 200˙000 gold nanorods per macrophage. Under these conditions, these cells are detectible by PAI down to concentrations in the order of 1% in whole blood and by CT below 10%, which is well below the typical fraction of a leukocytic infiltrate in a TME. Moreover, these cells hold the potential to serve as contrast agents for the optical hyperthermia of cancer as well.

In the future, we will take the challenge to translate these results in vivo and to make a critical comparison with the conventional approach to deliver plasmonic particles to tumors, which is their PEGylation, bio-conjugation[20, 24, 30, 31] and direct infusion into the bloodstream. Indeed, while tumor-tropic cells exhibit an unique ability to cross all biological barriers before their target much better than any artificial bullet, their actual biodistribution upon modification and reinjection into a full body remains an open question. In this context, we believe that the perspective to reproduce these results with complementary kinds of tumor-tropic cells, including T cells and stem cells, represents a remarkable opportunity.

4. Experimental Section

Preparation of Polycationic Gold Nanorods: Chemicals were purchased from Sigma-Aldrich (St. Louis, MO, USA) and used as received. The preparation of polycationic gold nanorods began with the synthesis of cetrimonium-capped gold nanorods by the autocatalytic reduction

of chloroauric acid with ascorbic acid, according to our variant[78] of the method by Nikoobakht et al[79]. These particles were purified by centrifugation and transferred at a concentration of 1.8 mM Au into a 100 mM acetate buffer at pH 5 containing Cetyltrimethylammonium Bromide (CTAB, 500 µM) and polysorbate 20 (50 ppm). In a typical run, an aliquot of this suspension (6 mL) was added with aqueous alpha-methoxy-omega-mercapto-PEG (MW ~ 5000, 30 µL, 10 mM), left to react for 30 minutes at 37 °C, added with MUTAB (30 µL, 100 mM in dimethyl sulfoxide) and left at rest for another 24 hrs at 37°C. Finally, these particles were purified by centrifugation and stored at a concentration of 4.5 mM Au in sterile PBS at pH 7.4 until use.

Preparation of Plasmonic Macrophages: J774a.1 monocyte/macrophagic cells were purchased from the American Type Culture Collection (ATCC® TIB-67™, Manassas, VA, USA) and seeded on plastic culture dishes in Dulbecco's Modified Eagle Medium (DMEM) supplemented with fetal bovine serum (10%), L-glutamine (1%) and a penicillin-streptomycin solution (1%) (BioWhittaker®, Lonza, Visp, Switzerland). Cells were kept and left to grow under standard culture conditions (37°C, 5% CO_2).

In a typical run, an appropriate number of macrophages was cultured in complete medium for 24 hrs and then incubated in serum-free medium to maintain starvation. Appropriate aliquots of polycationic gold nanorods in PBS were diluted in serum-free medium, so as to achieve the final concentration of choice and left in incubation for the duration of choice.

Quantitative Measurement of Intracellular Uptake: The accumulation of gold nanorods in macrophages was quantified by an optical analysis[24, 63, 64]. 5×10^5 J774a.1 cells were plated in Petri dishes and treated with different concentrations of gold nanorods (4, 10, 40, 100 and 400 µM Au) for 24 hrs or with 100 and 400 µM Au for different durations (0.5, 1, 2, 4, 8, 16 and 24 hrs). Macrophages were harvested, thoroughly rinsed with PBS and fixed with paraformaldehyde (3.6% in PBS) for 10 minutes at room temperature. Then their pellets were

washed, re-suspended in PBS (120 μL), transferred into a quartz micro-cuvette and directed to a UV-NIR spectrophotometer (V-560, Jasco, Tokyo, Japan).

Measurement of Cellular Viability and Chemotaxis: Cellular viability was evaluated by a WST-8 assay (Cell counting kit-8, Sigma-Aldrich, St. Louis, MO, USA). The highly water-soluble tetrazolium salt WST-8 is reduced by dehydrogenases within cells, which generates the yellow product formazan. The optical absorbance of formazan at 460 nm is proportional to the number of living cells. 8×10^3 macrophages were cultured in 96-well plates and incubated with 50, 100, 200 e 400 μM Au for 4, 24 and 48 hrs. Each sample was prepared in triplicate. At the end of the treatment, each well was washed with abundant PBS and cells were incubated with serum-free medium (100 μL) supplemented with WST-8 (10%) for 2 to 4 hrs at 37°C. The optical absorbance of formazan was quantified by a microplate reader (LT-400, Labtech, Bergamo, Italy) at 460 nm with a reference at 630 nm. Data were expressed as the percentage of signal with respect to controls.

A migration assay was implemented by the use of 24-well plates with polycarbonate membrane inserts (8 μm pore size, Transwell® Permeable Supports, Costar®, Corning Life Sciences, Lowell, MA, USA). Confluent macrophages were incubated in serum-free medium and then treated with 100 and 400 μM Au for 24 hrs. Thereafter 2.5×10^4 cells were harvested, re-suspended in serum-free medium (100 μL) and added to the upper side of the inserts. The lower well was filled with serum-free medium (600 μL) with or without MIP-1α (50 ng mL^{-1}) in the presence of bovine serum albumin (0.1%). These plates were left at 37°C overnight. Thereafter non-migrated cells remaining on the upper side of the inserts were removed with a cotton swab. Migrated cells were fixed with a paraformaldehyde (3.6% in PBS) for 10 minutes at room temperature and stained with Harris' hematoxylin and eosin. Each insert was observed by a light microscope at 40× magnification and migrated cells were quantified as means ± SD in 5 random fields.

Photoacoustic and CT imaging: Photoacoustic measurements were performed with a photoacoustic system from VisualSonics Inc. (Vevo LAZR, VisualSonics Inc., Toronto, Canada) that produces photoacoustic images co-registered with B-mode US images. A full description of the system is available in ref [73]. Photoacoustic signals were excited by a pulsed (20 Hz repetition, 6 to 8 ns pulse duration) and tunable (680 to 970 nm wavelength) Nd: YAG laser-pumped optical parametric oscillator through two rectangular fiber-optic bundles placed on both sides of a linear array transducer (13 to 24 MHz bandwidth, 23 mm × 30 mm field of view size) at an angle of 30° of the image plane. The acquisition time for a photoacoustic spectrum was about 60 s for 146 wavelength points.

A plastic device hosting 6 micro-channels (μ-Slide $VI^{0.1}$, Ibidi GmbH, Planegg, Germany) filled with different samples was used for photoacoustic measurements (**Figure 5a**). A 5 mm layer of tissue-like material composed of polydimethylsiloxane (PDMS) mixed with TiO_2 (0.73 mg mL^{-1}) and India ink (0.25 mg mL^{-1}) was deposited onto this device in order to gain more biomedical relevance and to prevent the gold nanorods to overheat upon irradiation[80]. A full description of the tissue-like material is reported elsewhere[81]. Spectra of optical absorbance were acquired from different dilutions of gold nanorods and different formulations of plasmonic macrophages that were either dispersed in PBS or in human whole blood.

In order to acquire CT scans, we used an IRIS scanner, which is a novel multimodal preclinical tomograph for high resolution PET/CT imaging of small animals (Raytest, Inviscan Imaging System, Strasbourg, France). The CT section is equipped with a microfocus X-ray source (35 to 80 kV voltage, 80 W power) with fixed tungsten anode and nominal maximum focal spot size of 50 μm and with a flat-panel CMOS-based X-ray detector coupled to a CsI: Tl scintillator with a thickness of 150 μm. The detector is divided into 1536 × 1944 square pixels (transaxial × longitudinal) with side length of 75 μm, for a total active surface of 115 mm × 145 mm. At full resolution, the minimum exposure time per frame in sequence mode is 39 ms, which can be shortened to 15 ms and 12 ms by 2 × 2 and 4 × 4 hardware

rebinning, respectively. The nominal source-to-axis distance (SAD) and source-to-detector distance (SDD) are 206 mm and 262 mm, respectively, which results into a transaxial field of view diameter of 90 mm. Images are reconstructed by a Feldkamp-type filtered back-projection algorithm and calibrated in Hounsfield units (H.U.).

A 96-well plate containing different samples was used for CT measurements (**Figure 5b**). The optimization of the CT signal as a function of voltage was carried out with a clinical CT scan in the range of clinical relevance between 80 and 120 kV. Thereafter, 80 kV was chosen as the optimal voltage for CT acquisitions of samples containing gold nanorods by the IRIS scanner (80 μm voxel size, 1 mA current, 1280 n. of views and ~ 60 s acquisition time).

Supporting Information

Supporting Information is available from the Wiley Online Library or from the author.

Acknowledgements

This work has been partially supported by the Project of Tuscan Region "NANOTREAT" and by the ERANET+ Project of Tuscan Region and European Community "LUS BUBBLE". The authors wish to thank Dr. Daniele Panetta for his expertise in X-ray microimaging.

Received: ((will be filled in by the editorial staff))

Revised: ((will be filled in by the editorial staff))

Published online: ((will be filled in by the editorial staff))

[1] X. Yang, M. Yang, B. Pang, M. Vara, Y. Xia, *Chem. Rev.* **2015**, *115*, 10410-88.

[2] C. C. Bao, N. Beziere, P. del Pino, B. Pelaz, G. Estrada, F. R. Tian, V. Ntziachristos, J. M. de la Fuente, D. X. Cui, *Small* **2013**, *9*, 68-74.

[3] E. C. Dreaden, A. M. Alkilany, X. H. Huang, C. J. Murphy, M. A. El-Sayed, *Chem. Soc. Rev.* **2012**, *41*, 2740-79.

[4] L. C. Kennedy, L. R. Bickford, N. A. Lewinski, A. J. Coughlin, Y. Hu, E. S. Day, J. L. West, R. A. Drezek, *Small* **2011**, *17*, 169-83.

[5] F. Ratto, P. Matteini, S. Centi, F. Rossi, R. Pini, *J. Biophoton.* **2011**, *4*, 64-73.

[6] J. Y. Chen, M. X. Yang, Q. A. Zhang, E. C. Cho, C. M. Cobley, C. Kim, C. Glaus, L. H. V. Wang, M. J. Welch, Y. N. Xia, *Adv. Funct. Mater.* **2010**, *20*, 3684-94.

[7] P. J. van den Berg, K. Daoudi, W. Steenbergen, *Photoacoustics* **2015**, *3*, 89-99.

[8] L. V. Wang, *Nature Photon.* **2009**, *3*, 503-9.

[9] A. M. Alkilany, L. B. Thompson, S. P. Boulos, P. N. Sisco, C. J. Murphy, *Adv. Drug Deliv. Rev.* **2012**, *64*, 190-9.

[10] N. Khlebtsov, L. Dykman, *Chem. Soc. Rev.* **2011**, *40*, 1647-71.

[11] N. Lewinski, V. Colvin, R. Drezek, *Small* **2008**, *4*, 26-49.

[12] P. K. Jain, K. S. Lee, I. H. El-Sayed, M. A. El-Sayed, *J. Phys. Chem. B* **2006**, *110*, 7238-48.

[13] H. J. Chen, L. Shao, Q. Li, J. F. Wang, *Chem. Soc. Rev.* **2013**, *42*, 2679-724.

[14] L. Vigderman, B. P. Khanal, E. R. Zubarev, *Adv. Mater.* **2012**, *36*, 4811-41.

[15] J. Perez-Juste, I. Pastoriza-Santos, L. M. Liz-Marzan, P. Mulvaney, *Coord. Chem. Rev.* **2005**, 249, 1870-901.

[16] S. Kessentini, D. Barchiesi, *Biomed. Opt. Expr.* **2012**, *3*, 590-604.

[17] G. von Maltzahn, J. H. Park, A. Agrawal, N. Kishor Bandaru, S. K. Das, M. J. Sailor, S. N. Bhatia, *Cancer Res.* **2009**, *69*, 3892-900.

[18] M. Mazzoni, F. Ratto, C. Fortunato, S. Centi, F. Tatini, R. Pini, *J. Phys. Chem. C* **2014**, *118*, 20018-25.

[19] P. P. Joshi, S. J. Yoon, Y. S. Chen, S. Emelianov, K. V. Sokolov, *Biomed. Opt. Expr.* **2013**, *4*, 2609-18.

[20] C. Ungureanu, R. Kroes, W. Petersen, T. A. M. Groothuis, F. Ungureanu, H. Janssen, F. W. B. van Leeuwen, R. P. H. Kooyman, S. Manohar, T. G. van Leeuwen, *Nano Lett.* **2011**, *11*, 1887-94.

[21] J. V. Jokerst, M. Thangaraj, P. J. Kempen, R. Sinclair, S. S. Gambhir, *ACS Nano* **2012**, *6*, 5920-30.

[22] Y. Huang, F. Rosei, F. Vetrone, *Nanoscale* **2015**, *7*, 5178-85.

[23] G. Terentyuk, E. Panfilova, V. Khanadeev, D. Chumakov, E. Genina, A. Bashkatov, V. Tuchin, A. Bucharskaya, G. Maslyakova, N. Khlebtsov, B. Khlebtsov, *Nano Res.* **2014**, *7*, 325-37.

[24] F. Ratto, E. Witort, F. Tatini, S. Centi, L. Lazzeri, F. Carta, M. Lulli, D. Vullo, F. Fusi, C. T. Supuran, A. Scozzafava, S. Capaccioli, R. Pini, *Adv. Funct. Mater.* **2015**, *25*, 316-23.

[25] F. Tatini, I. Landini, F. Scaletti, L. Massai, S. Centi, F. Ratto, S. Nobili, G. Romano, F. Fusi, L. Messori, E. Mini, R. Pini, *J. Mater. Chem. B* **2014**, *2*, 6072-80.

[26] T. Niidome, M. Yamagata, Y. Okamoto, Y. Akiyama, H. Takahashi, T. Kawano, Y. Katayama, Y. Niidome, *J. Control. Release* **2006**, 114, 343-7.

[27] X. H. Huang, X. H. Peng, Y. Q. Wang, Y. X. Wang, D. M. Shin, M. A. El-Sayed, S. M. Nie, *ACS Nano* **2010**, *4*, 5887-96.

[28] Y. Akiyama, T. Mori, Y. Katayama, T. Niidome, *J. Control. Release* **2009**, *139*, 81-4.

[29] S. D. Perrault, C. Walkey, T. Jennings, H. C. Fischer, W. C. W. Chan, *Nano Lett.* **2009**, *9*, 1909-15.

[30] S. Centi, F. Tatini, F. Ratto, A. Gnerucci, R. Mercatelli, G. Romano, I. Landini, S. Nobili, A. Ravalli, G. Marrazza, E. Mini, F. Fusi, R. Pini, *J. Nanobiotech.* **2014**, *12*, 55.

[31] B. C. Rostro-Kohanloo, L. R. Bickford, C. M. Payne, E. S. Day, L. J. Anderson, M. Zhong, S. Lee, K. M. Mayer, T. Zal, L. Adam, C. P. Dinney, R. A. Drezek, J. L. West, J. H. Hafner, *Nanotechnology* **2009**, *20*, 434005.

[32] C. Ayala-Orozco, C. Urban, M. W. Knight, A. Skyrme Urban, O. Neumann, S. W. Bishnoi, S. Mukherjee, A. M. Goodman, H. Charron, T. Mitchell, M. Shea, R. Roy, S. Nanda, R. Schiff, N. J. Halas, A. Joshi, *ACS Nano* **2014**, *6*, 6372-81.

[33] P. Puvanakrishnan, J. Park, D. Chatterjee, S. Krishnan, J. W. Tunnell, *Int. J. Nanomed.* **2012**, *7*, 1251-8.

[34] S. K. Sriraman, B. Aryasomayajula, V. P. Torchilin, *Tissue Barriers* **2014**, *2*, e29528.

[35] A. J. Trinidad, S. J. Hong, Q. Peng, S. J. Madsen, H. Hirschberg, *Lasers Surg. Med.* **2014**, *46*, 310-8.

[36] M. R. Choi, R. Bardhan, K. J. Stanton-Maxey, S. Badve, H. Nakshatri, K. M. Stantz, N. Cao, N. J. Halas, S. E. Clare, *Cancer Nano* **2012**, *3*, 47-54.

[37] T. D. Yang, W. Choi, T. H. Yoon, K. J. Lee, J. S. Lee, S. H. Han, M. G. Lee, H. S. Yim, K. M. Choi, M. W. Park, *J. Biomed. Opt.* **2012**, *17*, 128003.

[38] S. J. Madsen, S. K. Baek, A. R. Makkouk, T. Krasieva, H. Hirschberg, *Ann. Biomed. Eng.* **2012**, *40*, 507-15.

[39] M. R. Choi, K. J. Stanton-Maxey, J. K. Stanley, C. S. Levin, R. Bardhan, D. Akin, S. Badve, J. Sturgis, J. P. Robinson, R. Bashir, N. J. Halas, S. E. Clare, *Nano Lett.* **2007**, 7, 3759-65.

[40] L. C. Kennedy, A. S. Bear, J. K. Young, N. A. Lewinski, J. Kim, A. E. Foster, R. A. Drezek, *Nanoscale Res. Lett.* **2011**, *6*, 283.

[41] L. Pascucci, V. Coccè, A. Bonomi, D. Ami, P. Ceccarelli, E. Ciusani, L. Viganò, A. Locatelli, F. Sisto, S. M. Doglia, E. Parati, M. E. Bernardo, M. Muraca, G. Alessandri, G. Bondiolotti, A. Pessina, *J. Control. Release* **2014**, *192*, 262-70.

[42] J. Zhao, J. Vykoukal, M. Abdelsalam, A. Recio-Boiles, Q. Huang, Y. Qiao, B. Singhana, M. Wallace, R. Avritscher, M. P. Melancon, *Nanotechnology* **2014**, *25*, 405101.

[43] L. Li, Y. Guan, H. Liu, N. Hao, T. Liu, X. Meng, C. Fu, Y. Li, Q. Qu, Y. Zhang, S. Ji, L. Chen, D. Chen, F. Tang, *ACS Nano* **2011**, *5*, 7462-70.

[44] R. Mooney, L. Roma, D. Zhao, D. Van Haute, E. Garcia, S. U. Kim, A. J. Annala, K. S. Aboody, J. M. Berlin, *ACS Nano* **2014**, *8*, 12450-60.

[45] K. Schnarr, R. Mooney, Y. Weng, D. Zhao, E. Garcia, B. Armstrong, A. J. Annala, S. U. Kim, K. S. Aboody, J. M. Berlin, *Adv. Healthcare Mater.* **2013**, *2*, 976-82.

[46] S. Tan, T. Wu, D. Zhang, Z. Zhang, *Theranostics* **2015**, *5*, 863-81.

[47] R. Noy, J. W. Pollard, *Immunity* **2014**, *41*, 49-61.

[48] P. Barcellos-de-Souza, V. Gori, F. Bambi, P. Chiarugi, *Biochim. Biophys. Acta* **2013**, 1836, 321-35.

[49] P. Chiarugi, *Oncoimmunology* **2013**, *2*, e25563.

[50] A. Mantovani, P. Allavena, *J. Exp. Med.* **2015**, *212*, 435-45.

[51] R Weissleder, M Nahrendorf, MJ Pittet, *Nature Mater.* **2014**, *13*, 125-38.

[52] J. B. Mitchem, D. J. Brennan, B. L. Knolhoff, B. A. Belt, Y. Zhu, D. E. Sanford, L. Belaygorod, D. Carpenter, L. Collins, D. Piwnica-Worms, S. Hewitt, G. M. Udupi, W. M. Gallagher, C. Wegner, B. L. West, A. Wang-Gillam, P. Goedegebuure, D. C. Linehan, D. G. DeNardo, *Cancer Res.* **2013**, *73*, 1128-41.

[53] R. Z. Panni, D. C. Linehan, D. G. DeNardo, *Immunotherapy* **2013**, *5*, 1075-87.

[54] B. Wang, E. Yantsen, T. Larson, A. B. Karpiouk, S. Sethuraman, J. L. Su, K. Sokolov, S. Y. Emelianov, *Nano Lett.* **2009**, *9*, 2212-7.

[55] C. E. Lewis, R. Leek, A. Harris, J. O. McGee, *J. Leukoc. Biol.* **1995**, *57*, 747-51.

[56] C. O'Sullivan, C. E. Lewis, *J. Pathol.* **1994**, *172*, 229-35.

[57] D. A. Loeffler, P. C. Keng, R. B. Baggs, E. M. Lord, *Int. J. Cancer* **1990**, *45*, 462-7.

[58] L. Vigderman, P. Manna, E. R. Zubarev, *Angew. Chem. Int. Ed.* **2012**, *51*, 636-41.

[59] T. S. Hauck, A. A. Ghazani, W. C. W. Chan, *Small* **2008**, *4*, 153-8.

[60] E. Oh, J. B. Delehanty, K. E. Sapsford, K. Susumu, R. Goswami, J. B. Blanco-Canosa, P. E. Dawson, J. Granek, M. Shoff, Q. Zhang, P. L. Goering, A. Huston, I. L. Medintz, *ACS Nano* **2011**, *5*, 6434-48.

[61] J. B. Delehanty, K. Boeneman, C. E. Bradburne, K. Robertson, J. E. Bongard, I. L. Medintz, *Ther. Deliv.* **2010**, *1*, 411-33.

[62] H. Yuan, A. M. Fales, T. Vo-Dinh, *J. Am. Chem. Soc.* **2012**, *134*, 11358-61.

[63] P. Matteini, F. Ratto, F. Rossi, M. de Angelis, L. Cavigli, R. Pini, *J. Biophotonics* **2012**, *5*, 868-77.

[64] F. Ratto, P. Matteini, A. Cini, S. Centi, F. Rossi, F. Fusi, R. Pini, *J. Nanopart. Res.* **2011**, *13*, 4337-48.

[65] P. G. Etchegoin, E. C. Le Ru, M. Meyer, *J. Chem. Phys.* **2006**, *125*, 164705.

[66] P. Menten, A. Wuyts, J. Van Damme, *Cytok. Growth Factor Rev.* **2002**, *13*, 455-81.

[67] E. I. Galanzha, D. A. Nedosekin, M. Sarimollaoglu, A. I. Orza, A. S. Biris, V. V. Verkhusha, V. P. Zharov, *J. Biophotonics* **2015**, *8*, 81-93.

[68] V. P. Zharov, *Nat. Photonics* **2011**, *5*, 110-6.

[69] H. Ju, R. A. Roy, T. W. Murray, *Biomed. Opt. Express* **2012**, *4*, 66-76.

[70] E. Y. Lukianova-Hleb, X. Y. Ren, R. R. Sawant, X. W. Wu, V. P. Torchilin, D. O. Lapotko, *Nat. Med.* **2014**, *20*, 778-84.

[71] E. Lukianova-Hleb, Y. Hu, L. Latterini, L. Tarpani, S. Lee, R. A. Drezek, J. H. Hafner, D. O. Lapotko, *Nano Lett.* **2010**, *4*, 2109-23.

[72] R. K. Saha, M. C. Kolios, *J. Biomed. Opt.* **2011**, 16, 115003.

[73] A. Needles, A. Heinmiller, P. Ephrat, C. Bilan-Tracey, A. Trujillo, C. Theodoropoulos, D. Hirson, F. S. Foster, *2010 IEEE Int. Ultrasonics Symp. Proc.* **2010**, 390-3.

[74] C. Iodice, A. Cervadoro, A. Palange, J. Key, S. Aryal, M. R. Ramirez, C. Mattu, G. Ciardelli, B. E. O'Neill, P. Decuzzi, *Opt. Laser Eng.* **2016**, *76*, 74-81.

[75] Z. W. Li, S. N. Yin, L. Cheng, K. Yang, Y. G. Li, Z. Liu, *Adv. Funct. Mater.* **2014**, *24*, 2312-21.

[76] X. H. Huang, P. K. Jain, I. H. El-Sayed, M. A. El-Sayed, *Lasers Med. Sci.* **2008**, *23*, 217-28.

[77] B. Khlebtsov, V. Zharov, A. Melnikov, V. Tuchin, N. Khlebtsov, *Nanotechnology* **2006**, *17*, 5167-79.

[78] F. Ratto, P. Matteini, F. Rossi, R. Pini, *J. Nanopart. Res.* **2009**, *12*, 2029-36.

[79] B. Nikoobakht, M. A. El-Sayed, *Chem. Mater.* **2003**, *15*, 1957-62.

[80] L. Cavigli, M. de Angelis, F. Ratto, P. Matteini, F. Rossi, S. Centi, F. Fusi, R. Pini, *J. Phys. Chem. C* **2014**, *118*, 16140-6.

[81] C. Avigo, N. Di Lascio, P. Armanetti, C. Kusmic, L. Cavigli, F. Ratto, S. Meucci, C. Masciullo, M. Cecchini, R. Pini, F. Faita, L. Menichetti, *J. Biomed. Opt.* **2015**, *20*, 46008.

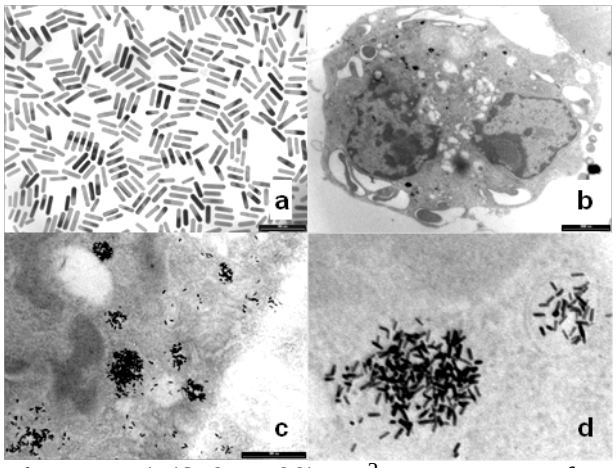

Figure 1. a) (650 × 500) nm^2 TEM image of as-synthesized gold nanorods; b), c) and d) respectively (13 × 8.6) μm^2, (2.3 × 1.7) μm^2 and (870 × 650) nm^2 TEM images of macrophages grown on polycarbonate membranes and treated for 24 hrs with polycationic gold nanorods at a concentration of 400 µM Au, before fixation, inclusion in an epoxidic resin with their polycarbonate substrate and cutting into slices with a thickness of ~ 90 nm. The appearance of the particles in panel (d) is affected by their inclination in the macrophagic cells.

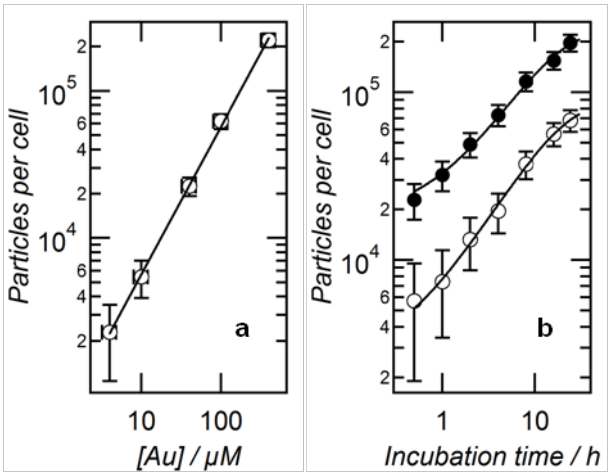

Figure 2: Number of polycationic gold nanorods that are taken up per macrophagic cell treated in (a) for 24 hrs at different concentrations of gold and in (b) for different incubation times with 100 (empty circles) and 400 (full circles) μM Au. Data were retrieved from an optical analysis of aqueous suspensions of these cells and expressed as average ± standard deviation of three independent runs.

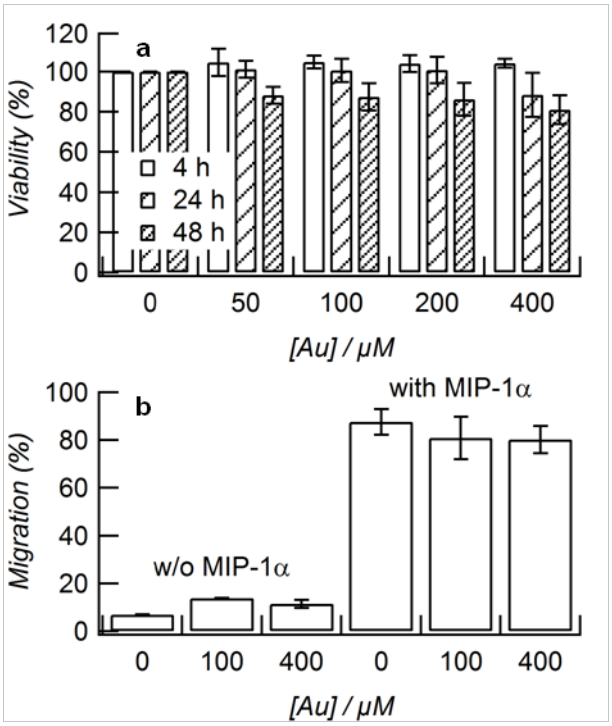

Figure 3: a) Viability of macrophagic cells treated for different incubation times with different concentrations of gold and retrieved from a WST-8 assay. Data are expressed as percent of formazan with respect to controls. Values are reported as mean ± SD of three independent experiments; b) percent of macrophages treated for 24 hrs with different concentrations of gold that migrated after exposure to MIP-1α with respect to controls. The chemotaxis assay was performed by the use of Transwell® permeable membranes. Results are shown as mean ± SD of three independent experiments.

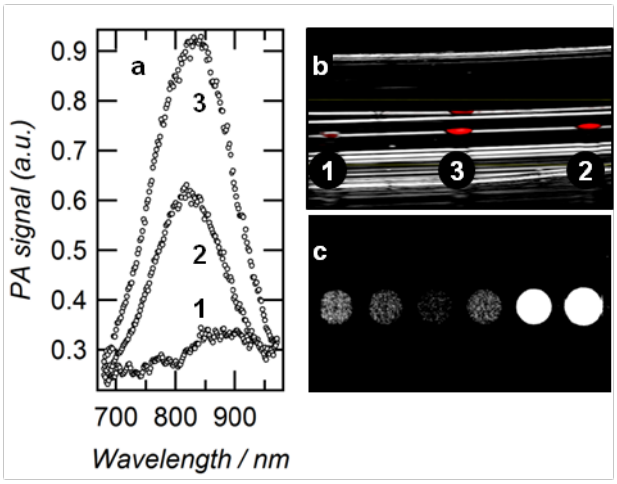

Figure 4: a) Photoacoustic spectra and b) (2.1 × 1.2) cm^2 combined B-mode ultrasound (grey) and photoacoustic (red) image at an optical wavelength of 820 nm of three micro-channels that were filled with human whole blood (1), a suspension of gold nanorods in whole blood at the concentration of 1 mM Au (2) and whole blood containing ~3% (v/v) macrophages treated for 24 hrs with 400 µM Au (3); c) CT image of a set of inclusions containing, from left to right, ~ 8% (v/v) macrophagic cells treated for 24 hrs with 400 µM Au, a suspension of gold nanorods at the concentration of 4 mM Au, PBS and increasing dilutions of iodine in PBS (3.2, 32 and 320 mM I).

Figure 5: a) photograph of a plastic device with three of its six micro-channels filled with blood and two different dilutions of gold nanorods in blood; b) photograph of a 96-well plate filled with different dilutions of gold nanorods in PBS.

Hybrid particles with plasmonic bands in the near infrared are engineered to undergo consistent uptake from tumor-tropic cells, without affecting their viability and chemotaxis. These cells may be recruited as Trojan horses to target tumors across all biological barriers and to enable their multimodal detection by photoacoustic imaging and X-ray computed tomography and their destruction by photothermal ablation.

Nanomedicine

Fulvio Ratto*, Sonia Centi, Cinzia Avigo, Claudia Borri, Francesca Tatini, Lucia Cavigli, Claudia Kusmic, Beatrice Lelli, Sarah Lai, Stefano Colagrande, Francesco Faita, Luca Menichetti and Roberto Pini

A Robust Design for Cellular Vehicles of Gold Nanorods for Multimodal Imaging

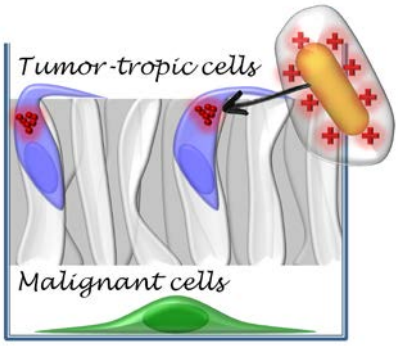

Supporting Information

A Robust Design for Cellular Vehicles of Gold Nanorods for Multimodal Imaging

Fulvio Ratto, Sonia Centi, Cinzia Avigo, Claudia Borri, Francesca Tatini, Lucia Cavigli, Claudia Kusmic, Beatrice Lelli, Sarah Lai, Stefano Colagrande, Francesco Faita, Luca Menichetti and Roberto Pini*

Optical micrographs of the macrophages

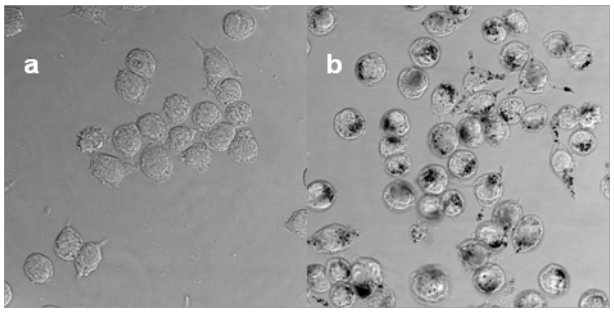

Figure S1: optical transmission micrographs of a) blank macrophagic cells and b) macrophagic cells treated for 24 hrs with 400 µM Au.

Figure S1 is representative of the appearance under an optical microscope of control macrophages and macrophages treated for 24 hrs with 400 µM Au. The morphology of these cells is retained after the treatment. The uptake of gold nanorods occurs by the extroflession of pseudopodia and their accumulation is evident from a pattern of dark vesicles inside the perinuclear cytoplasm.

Spectra of optical extinction from the macrophages

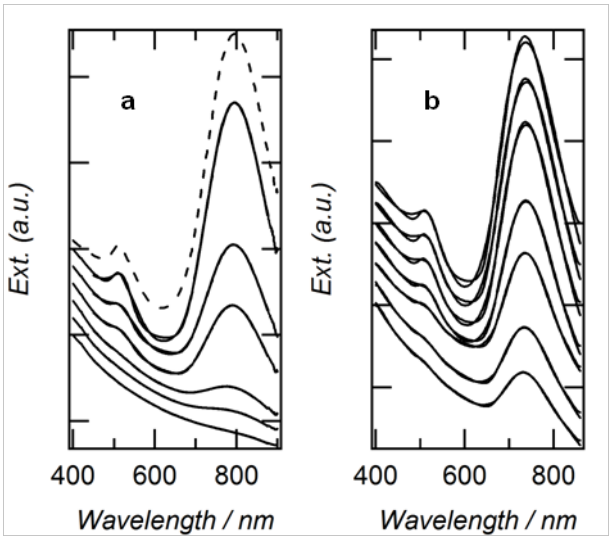

Figure S2: representative sets of spectra of optical extinction of macrophagic cells treated in (a) for 24 hrs w/out and with 4, 10, 40, 100 and 400 µM Au, from bottom to top, and in (b) for 30 min and 1, 2, 4, 8, 16 and 24 hrs with 400 µM Au, from bottom to top. All spectra were fitted and overlaid with the lineshape that is described in the main text. The agreement between the experimental data and their analytical representation is excellent. The dashed line in panel (a) refers to a colloidal suspension of as-synthesized gold nanorods. All spectra were offset for clarity.

Figure S2 shows examples of the spectra of optical extinction of macrophages treated for 24 hrs with different concentrations of gold in panel (a) and for different incubation times with 400 µM Au in panel (b). The spectrum of the as-synthesized gold nanorods that were used in panel (a) is represented by the dashed line and is given to prove the near-absence of relevant modifications upon internalization. All spectra were fitted to a theoretical lineshape that is described in refs [24, 63, 64]. The agreement between the experimental data and their theoretical description is remarkable, which corroborates the near-absence of plasmonic coupling. For the sake of clarity, all spectra were offset.

Spectra and calibration of photoacoustic signals

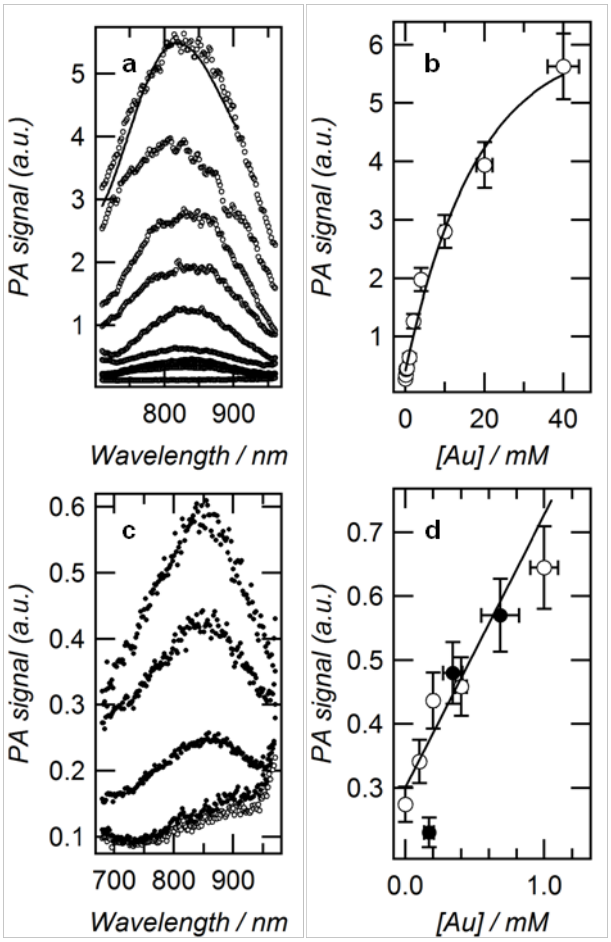

Figure S3: a) photoacoustic spectra of PBS and suspensions of polycationic gold nanorods at the concentrations of 0.1, 0.2, 0.4, 1, 2, 4, 10, 20 and 40 mM Au in PBS, from bottom to top. The continuous line represents the spectrum of optical extinction of these particles and is reported for the sake of comparison; b) calibration curve from the data in panel (a); c) photoacoustic spectra of PBS and suspensions of 10^7 blank macrophages per cc and 10^7 macrophages per cc that were treated with 100, 200 and 400 µM Au, from bottom to top; d) close-up of the calibration curve in panel (b) (open circles), which was overlaid with the data from panel (c) (full circles), upon consideration of the cargo of particles per cell from **Figure 2a**.

Figure S3 summarizes our results on the identification of our particles by photoacoustic spectroscopy. Panel (a) reports the PA spectra of suspensions containing different concentrations of gold. The continuous line is a spectrum of optical extinction of these particles and is reproduced in order to illustrate its correlation with the photoacoustic spectra. Panel (b) is the relevant calibration curve, which points to a detection limit in the order of 100 µM Au. Panel (c) contains the photoacoustic spectra of PBS, 10^7 blank macrophages per cc and 10^7 macrophages per cc that were treated with different concentrations of gold. The plasmonic band is retraced well even in these samples. Finally, panel (d) is a close-up of panel (b), where the full circles were added to represent the data points from panel (c), by taking the numbers of particles per cell from **Figure 2a**.

Calibration of XR absorbance

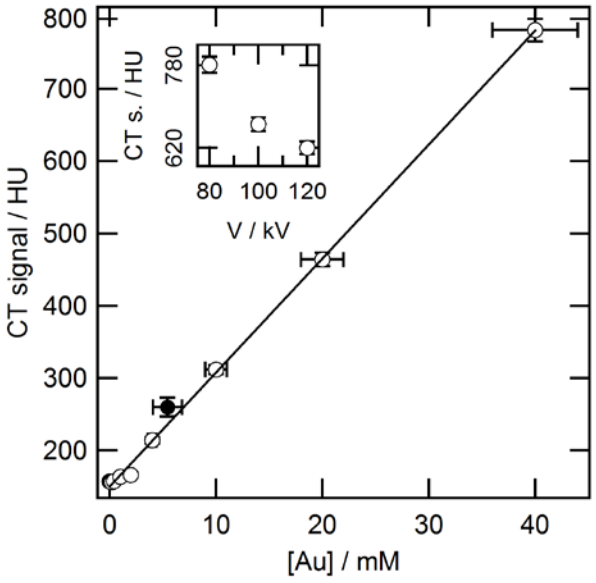

Figure S4: Absorbance of X rays as a function of the concentration of gold of different suspensions of polycationic gold nanorods (empty circles). The full circle refers to a suspension of ~ 8 × 10^7 macrophagic cells treated with 400 µM Au per cc, upon consideration of the load of particles per cell from **Figure 2a**. The inset shows a branch of the spectrum of

absorbance of X rays from a suspension of polycationic gold nanorods at the concentration of 40 mM Au.

Figure S4 reports the absorbance of X rays from our gold nanorods by the use of a CT device in clinical use. The inset displays our optimization of the CT signal as a function of voltage. In the range of clinical relevance between 80 and 120 kV, the absorbance of X rays from a suspension of gold nanorods is found to decrease by ~ 20%. The full circle represents the data point from a suspension containing ~ 8×10^7 macrophages treated with 400 µM Au per cc. Their gold content was estimated from **Figure 2a** and does not depart much from the calibration curve.

Photothermal ablation

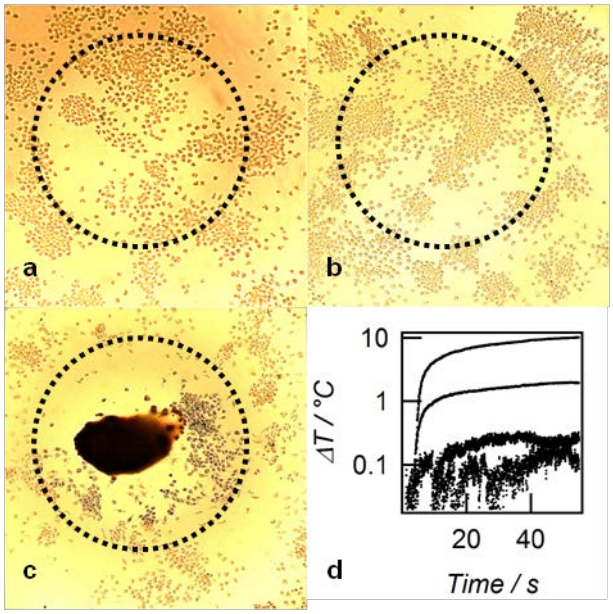

Figure S5: optical micrographs of blank macrophagic cells (a) and macrophagic cells treated for 24 hrs with 100 µM Au given in PEGylated gold nanorods[25] (b) and polycationic gold nanorods (c) after 15 minutes of optical excitation at 810 nm wavelength and 60 W cm^{-2} power density. All samples were stained with trypan blue; d) temperature below the Petri dish during the optical excitation of a monolayer of macrophagic cells treated for 24 hrs with 10

and 100 μM Au given in PEGylated gold nanorods and 10 and 100 μM Au in polycationic gold nanorods, from bottom to top.

Figure S5d reports the temperatures that were measured below a petri dish seeded with macrophages treated for 24 hrs with 10 and 100 μM Au given in PEGylated gold nanorods and with 10 and 100 μM Au in polycationic gold nanorods (from bottom to top) and excited from atop with a diode laser at the noninvasive power density of 60 W cm^{-2}. We warn the reader that the absolute values of these temperatures may consistently underestimate those in the overlaying cells, due to the dissipation of heat across the wall of the petri dish. After 15 minutes under these conditions, cells were treated with trypan blue, in order to highlight their death. Relevant micrographs are presented in panels (a) to (c), i.e. macrophages treated for 24 hrs with 100 μM Au given in polycationic gold nanorods, macrophages treated for 24 hrs with 100 μM Au in PEGylated gold nanorods and blank macrophages, respectively. We note that those cells that received the polycationic particles did not only undergo death but also aroused a significant damage to their substrate. In contrast, those cells that received PEGylated particles or no particles did not experience any harm.

[24] F. Ratto, E. Witort, F. Tatini, S. Centi, L. Lazzeri, F. Carta, M. Lulli, D. Vullo, F. Fusi, C. T. Supuran, A. Scozzafava, S. Capaccioli, R. Pini, *Adv. Funct. Mater.* **2015**, *25*, 316-23.

[25] F. Tatini, I. Landini, F. Scaletti, L. Massai, S. Centi, F. Ratto, S. Nobili, G. Romano, F. Fusi, L. Messori, E. Mini, R. Pini, *J. Mater. Chem. B* **2014**, *2*, 6072-80.

[63] P. Matteini, F. Ratto, F. Rossi, M. de Angelis, L. Cavigli, R. Pini, *J. Biophotonics* **2012**, *5*, 868-77.

[64] F. Ratto, P. Matteini, A. Cini, S. Centi, F. Rossi, F. Fusi, R. Pini, *J. Nanopart. Res.* **2011**, *13*, 4337-48.